Journal of Sol-Gel Science and Technology (2018) 86:617–630
https://doi.org/10.1007/s10971-018-4675-1

ORIGINAL PAPER: NANO-STRUCTURED MATERIALS (PARTICLES, FIBERS, COLLOIDS, COMPOSITES, ETC.)

Electrical and electrochemical characteristics of $La_{0.6}Sr_{0.4}CoO_{3-\delta}$ cathode materials synthesized by a modified citrate-EDTA sol-gel method assisted with activated carbon for proton-conducting solid oxide fuel cell application

Abdullah Abdul Samat[1] · Abdul Azim Jais[1] · Mahendra Rao Somalu[1] · Nafisah Osman[2] · Andanastuti Muchtar[1,3] · Kean Long Lim[1]

Received: 7 February 2018 / Accepted: 30 April 2018 / Published online: 17 May 2018

Abstract

The electrical conductivity and electrochemical performance of a $La_{0.6}Sr_{0.4}CoO_{3-\delta}$ (LSC) cathode produced by a modified citrate-EDTA sol-gel method assisted with activated carbon are characterized for a proton-conducting solid oxide fuel cell (H^+−SOFC) application at intermediate temperature. Thermogravimetric analysis revealed that the decomposition of the unrequired intermediate compounds in the precalcined powder was completed at 800 °C. A single LSC perovskite phase was formed at a calcination temperature of 900 °C, as confirmed by X-ray diffraction analysis. The particle size, crystallite size, and BET-specific surface area of the powder are 219–221 nm, 18 nm, and 9.87 $m^2 g^{-1}$, respectively. The high index value of the extent of agglomeration (5.53) showed that the powder was barely agglomerated. Bulk LSC sintered at 1200 °C for 2 h showed the highest direct-current electrical conductivity ($\sigma_{d.c}$) compared to that of bulk LSC sintered at 1000 °C and 1100 °C. The value of $\sigma_{d.c}$ was affected by the density and porosity of the sintered samples. The area specific resistance (ASR) of screen-printed LSC working on a proton conductor of $BaCe_{0.54}Zr_{0.36}Y_{0.1}O_{2.95}$ (BCZY) decreased from 5.0 Ω cm^2–0.06 Ω cm^2 as the temperature increased from 500 °C to 800 °C with an activation energy of 1.079 eV. Overall, in this work, the LSC material produced with the aid of activated carbon meet the requirements for the application as a cathode in an intermediate temperature H^+-SOFC.

Graphical Abstract

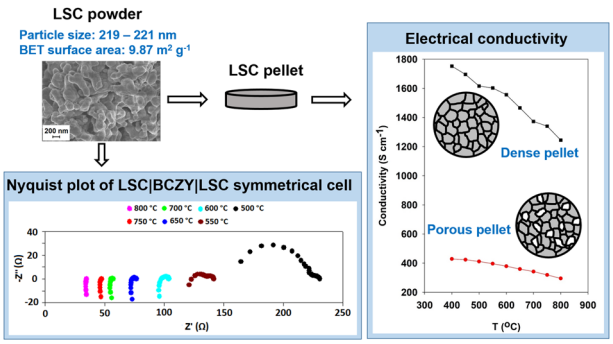

✉ Mahendra Rao Somalu
mahen@ukm.edu.my

[1] Fuel Cell Institute, Universiti Kebangsaan Malaysia, 43600 UKM Bangi, Selangor, Malaysia

[2] Faculty of Applied Sciences, Universiti Teknologi MARA, 02600 Arau, Perlis, Malaysia

[3] Centre for Materials Engineering and Smart Manufacturing (MERCU), Faculty of Engineering and Built Environment, Universiti Kebangsaan Malaysia, 43600 UKM Bangi, Selangor, Malaysia

Keywords: Solid oxide fuel cell · LSC cathode · Activated carbon · Sol-gel · Electrical properties

Highlights

- Activated carbon derived $La_{0.6}Sr_{0.4}CoO_{3-\delta}$ (LSC) has conductivity > 100 S cm^{-1}
- Electrical conductivity was affected by microstructure properties of LSC pellet
- Area specific resistance of LSC coupled with BCZY at 800 °C was 0.06 Ω cm^2
- LSC is a potential cathode material for proton-conducting solid oxide fuel cell

1 Introduction

Solid oxide fuel cells (SOFCs) have been attracting considerable attention worldwide as highly power generating devices due to their potential for high energy efficiency and zero/low environmental pollution. Traditionally, an SOFC must be operated at high temperatures (800–1000 °C) with the conventional electrolyte of yttria-stabilized zirconia (YSZ). At the high operating temperatures, some serious problems such as chemical and physical degradation of the SOFC components arise. Therefore, the development of SOFCs operating at intermediate temperatures (500–800 °C) is desirable. However, at reduced operating temperatures, the electrode polarization resistance increases and the electrolyte conductivity decreases, affecting the overall performance of the SOFCs. There are two approaches under active consideration to solve these problems. The first approach is the development of suitable cathode materials that can work at intermediate temperatures, and the second approach is the development of promising alternative electrolyte materials to replace the conventional YSZ electrolyte as it has low ionic conductivity at intermediate temperatures.

Strontium-doped lanthanum cobaltite, $La_{0.6}Sr_{0.4}CoO_{3-\delta}$ (LSC) is of great interest as a potential cathode material for intermediate temperature solid oxide fuel cells (IT-SOFCs). This material has shown good performance on both YSZ [1] and cerium gadolinium oxide, $Ce_{0.9}Gd_{0.1}O_{1.95}$ (GDC) [2, 3] electrolytes, which are oxide ion (O^{2-}) conducting electrolytes at intermediate temperatures. Furthermore, the LSC material is also used as a cathode component for IT-SOFCs that use yttrium-doped barium cerate-zirconate, $Ba(Ce,Zr)YO_3$, a proton (H^+) conducting electrolyte [4, 5]. A proton-conducting SOFC (H^+-SOFC) has a few remarkable advantages over the conventional oxide ion-conducting SOFC (O^{2-}-SOFC) such as low activation energy for charge transport, no fuel dilution and improved material compatibility.

Although LSC material is considered as a potential cathode candidate for an SOFC due to its intrinsic properties, modifying its microstructural properties may allow improved electrochemical performance. It is well known that the microstructural properties of a cathode material greatly depend on the processing routes used to produce the material. A promising and popular technique to produce cathode materials with excellent microstructural properties is a sol-gel method [6–8]. The well-known benefits of this technique are the high purity of powders with excellent stoichiometry control and high degree of homogeneity can be produced at relatively low processing temperatures. Additionally, this technique is also able to produce ultrafine powders of complex oxide compositions by controlling its processing parameters.

In the present work, a LSC cathode material was synthesized by a modified citrate-EDTA sol-gel method. Activated carbon (AC), which is a treated form of carbon, was used as a dispersing agent to replace the conventional solvent or surfactant, ethylene glycol (EG), due to its high degree of microporosity, surface area (300–2000 $m^2 g^{-1}$) and well-adsorption ability. The respective dispersing agent and surfactant are responsible for controlling the nucleation process, particle growth, and phase development during the synthesis process. To date, to the best of the authors' knowledge, there are only two studies that have reported the usage of AC in modifying the microstructural properties of the lanthanum cobaltite ($LaCoO_3$)-based cathode materials such as LSC [9, 10] and iron-doped LSC, $La_{0.6}Sr_{0.4}Co_{0.2}Fe_{0.8}O_{3-\delta}$ (LSCF) [7]. However, there are no detailed reports on the electrical conductivity and electrochemical performance of the cathode materials produced with AC as a dispersing agent, except for a LSCF cathode material that has been produced with the aid of carbon black as a dispersing agent [11]. Therefore, further evaluation of the effect of microstructural properties on the direct-current (d.c) conductivity of bulk LSC cathode powder produced by a modified sol-gel method assisted with AC is presented in this work. Additionally, the electrochemical performance between the LSC cathode and a proton conductor of $BaCe_{0.54}Zr_{0.36}Y_{0.1}O_{2.95}$ (BCZY) was also presented, as only a few studies have been reported in the literature, particularly for the LSC|BCZY|LSC system. The obtained results were systemically discussed to qualify the system as an alternative component for intermediate temperature H^+-SOFC applications.

2 Materials and methods

2.1 Sample preparation

Metal nitrate salt-based precursor materials with purity >99% (ACROS) were used to synthesis the LSC powder by

a modified citrate-EDTA sol-gel method assisted with AC. First, a metal nitrate salts solution was prepared by dissolving a stoichiometric amount of $La(NO_3)_3.6H_2O$, $Sr(NO_3)_2$, and $Co(NO_3)_2.6H_2O$ in deionized water. Second, a combined chelating agent comprising ethylenediaminetetraacetic acid (EDTA, 99% purity, ACROS) and citric acid (CA, 99.5% purity, Merck) was added into the metal nitrate salts solution. Then, an amount of ammonia hydroxide, NH_4OH (25% assays, HmbG® Chemicals) solution was added drop by drop to adjust the pH of the solution to a value of 0.5. Finally, an amount of AC was added into the solution mixture. The solution mixture was heated at 100 °C for several hours to evaporate the water, forming a viscous gel. The gel was dried at 150–250 °C and the obtained as-synthesized powder was then grounded and calcined at 900 °C for 5 h. The details of the production of the LSC powders were described elsewhere [9, 12].

The calcined powder was then pressed into 13-mm diameter pellets under isostatic pressure (5 tons, 1 min) using a hydraulic press machine (Carver, Model: 4350 L, IN, USA). The green pellets were sintered at different temperatures (1000, 1100, 1200 °C) with a rate of 5 °C min^{-1} to achieve a high relative density (>95%). Prior to the fabrication of the LSC film, the calcined LSC powder was mixed in a stoichiometric amount of acetone (solvent) and Hypermer KD15 (dispersant). The mixture was ball-milled in a zirconia jar using zirconia balls (diameter, 10 mm) for 5 h. The ratio of the LSC powder to the zirconia balls was 1:4. Next, the ball-milled LSC powder was dried at 90 °C in an oven for 6 h to evaporate the solvent. The dried powder was mixed with a solution of ethyl cellulose in terpineol and grounded in an agate mortar for 10 min. The mixture was then milled using a triple roll mill for 30 min to produce a homogenized LSC cathode ink. The prepared LSC cathode ink was then screen printed onto both surfaces of $BaCe_{0.54}Zr_{0.36}Y_{0.1}O_{2.95}$ (BZCY) electrolyte, to produce a symmetrical half-cell of LSC|BCZY|LSC. The symmetrical cell was then fired at 900 °C for 2 h.

2.2 Sample characterization

A thermogravimetric analysis instrument (TGA, Pyris Diamond TG/DTG analyzer, USA) was used to analyze the thermal decomposition behavior of the as-synthesized powder. Phase identification of the calcined LSC powder was done on an X-ray diffractometer (XRD, D8-Advance, Bruker, Germany) with nickel-filtered Cu-K_α radiation in the range of 20°–80° (2θ). Eqs. (1) and (2) were used to calculate the interplanar spacing (d) and lattice parameter (a) of the LSC particles, respectively.

$$d = \lambda/(2\sin\theta) \tag{1}$$

$$a = d\left[\sqrt{(h^2 + k^2 + l^2)}\right] \tag{2}$$

where λ is the wavelength of X-rays (Cu-$K_\alpha = 1.5406$ Å), θ is the Bragg angle and hkl are the Miller indices. The density (ρ) of the calcined LSC material was calculated using Eq. (3):

$$\rho = (n \times \mathrm{Mw})/(a^3 \times N_A) \tag{3}$$

where Mw is the molecular weight of the LSC, n refers to the number of atoms per unit cell and N_A is Avogadro's number (6.02×10^{23}). The crystallite size (D_{xrd}) of the LSC particles was calculated using Scherrer's Eq. (4):

$$D_{xrd} = k\lambda/(\beta\cos\theta) \tag{4}$$

where k refers to a factor of dimensionless shape (spherical shape = 0.9), λ is the Cu-K_α rays wavelength (0.15406 nm), θ is the Bragg angle in radians and β refers to the corrected full width at half maximum (FWHM). A BET surface area and porosity analyser (Micromeritics ASAP 2020, USA) was used to analyze the BET-specific surface area (S_v) of the calcined powder. The average particles size (D_{BET}) of the calcined LSC powder was calculated using Eq. (5) by assuming that the particles have a spherical shape.

$$D_{BET} = 6000/(\rho \times S_v) \tag{5}$$

where ρ is in g cm^{-3} and S_v is in m^2 g^{-1}. The images of the microstructure of the calcined powder were captured using Zeiss Supra-55 VP field emission scanning electron microscope (FESEM, Germany) and Philips CM-12 transmission electron microscope (TEM, USA). The mean particle size (D_{SEM}) was estimated by statistically analyzing 100 particles in the SEM photographs using ImageJ software. The sintered density values of the LSC pellets were performed by the Archimedes' method [13]. The microstructure images of the surface and the fractured cross section of the LSC pellets and symmetrical cells were captured by Hitachi U1510 scanning electron microscope (SEM, Japan).

The $\sigma_{d.c}$ was measured by the van der Pauw method using a Keithley 2400 combined current source (I = 100 mA) and voltmeter on the sintered LSC cathode pellets at temperatures between 500 °C and 800 °C in the presence of air flow (100 mL min^{-1}). Pt wires were used for the four electrodes in this measurement. The probe polarity or position was changed several times to measure the voltage values. Finally, the results were averaged and used to calculate the resistivity (R_s) and $\sigma_{d.c}$ values using Eqs. (6) and (7), respectively.

$$R_s = \pi R_{ave}/ln\,2 \tag{6}$$

$$\sigma_{d.c} = 1/R_s l \quad (7)$$

where R_{ave} is the average resistance and l is thickness of the sample. To determine the activation energy (E_a), the Arrhenius plots of ln (σT) vs. 1000/T were plotted and the experimental results were fitted to a straight line with the slope equal to $-E_a/1000k$ based on Eq. (8).

$$ln\,\sigma T = ln\,C - (E_a/kT) \quad (8)$$

where σ is the specific conductivity ($\sigma_{d.c}$), C is a material constant containing the carrier concentration term (S cm^{-1} K), T is the absolute temperature (in Kelvin) and k is Boltzmann's constant (8.617×10^{-5} eV K^{-1}). The alternating current (a.c) impedance measurement of the fabricated symmetrical cell was conducted in the presence of air flow (100 mL min^{-1}) at temperatures in the range of 500–800 °C at 50 °C intervals. The measurement was performed using an Autolab PGSTAT302N coupled with a frequency response analyser (Autolab 302, Eco Chemie, Netherlands) in a potentiostatic mode over a frequency range from 1.0^6–1.0^{-2} Hz with a sinusoidal voltage of 20 mV under an open circuit condition. Data obtained from the a.c impedance measurements were examined using NOVA software (Version 1.11). The a.c impedance diagrams were plotted in Z′ (real) versus Z′′ (imaginary) for the symmetrical cell. Eq. 9 was used to calculate the area specific resistance (ASR) of the LSC cathode.

$$\mathrm{ASR} = R_p A/2 \quad (9)$$

where R_p refers to the polarization resistance or resistance at cathode–electrolyte interface and A refers to the specific active area ($A = 1$ cm^2).

3 Results and discussion

3.1 Powder properties

The thermal decomposition behavior of the as-synthesized powder was studied to observe the multiple decomposition stages of organic and unrequired compounds until the desired oxide compound was obtained. Figure 1 presents the thermogravimetric curve of the as-synthesized LSC powder. The total weight loss was 83.76%. The decomposition started from 30 °C to 200 °C (Stage 1) with an initial weight loss of ~2.26% due to the dehydration of water or absorbed moisture and the elimination of remaining low boiling point (B_p) organic compounds such as CA ($B_p = 175$ °C), EG ($B_p = 197$ °C), and nitrate species ($B_p = 160$ °C) [6, 12]. A major weight loss of ~80.88% in the temperature region of 200–670 °C (Stage 2) is caused by the

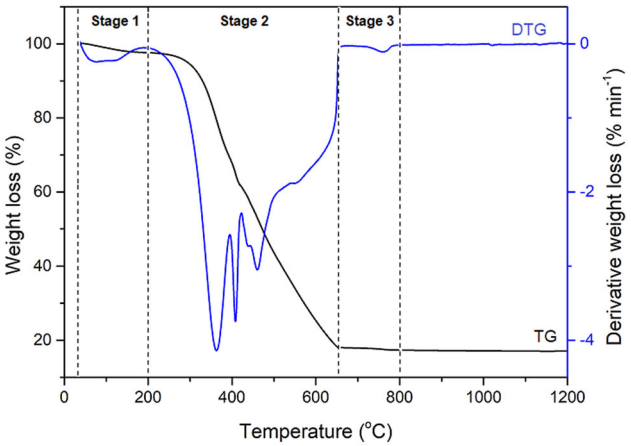

Fig. 1 TG/DTG curves of the as-synthesized $La_{0.6}Sr_{0.4}CoO_{3-\delta}$ powder

decomposition of residual nitrates and organics compounds (CA, EDTA, and AC) [11]. A minor weight loss of ~0.62% recorded at stage 3 in the temperature range between 670 °C and 800 °C corresponds to the decomposition of trapped carbonaceous residue [14, 15]. The TG signal became a plateau after stage 3 with no further weight loss, indicating that the desired oxide material may form in this region. Thus, the as-synthesized powder calcination was suggested to be calcined at temperatures above 800 °C.

Figure 2a displays the XRD pattern of the as-synthesized powder after it was calcined at a temperature of 900 °C. The sharpness in the XRD peaks indicated that the synthesized LSC is well crystalline after calcination, which agrees with the TGA result. The XRD measurement confirmed that the calcined powder formed a single LSC perovskite phase. All the peaks in the XRD spectrum were matched with the ICDD reference code 00-048-0121 (cubic structure, Pm-3m). The result is in line with our previous reported work [12] and comparable to other reported studies in the literature [2, 14, 16, 17]. The calculated lattice parameter (a) value of the single-phase LSC is 3.835 Å. The value is almost similar to the reference, i.e., 3.832 Å [18]. The calculated density (ρ) of the LSC powder is 6.31 g cm^{-3}, and the specific surface area is 9.87 m^2 g^{-1}. The estimated average crystallite sizes based on all the XRD peaks (D_{xrd}) and the BET surface area (D_{BET}) are 18 nm and 96 nm, respectively. The large difference between the values of D_{xrd} and D_{BET} indicates the partial sintering of the active nanocrystallites to form agglomerates [19]. It is well known that the major disadvantage of wet chemical methods including sol-gel is the formation of hard agglomerates of the ultrafine crystallites or particles. Therefore, the index value of agglomeration extent (ψ), which is defined as a factor that reflects the agglomeration extent of the 'primary' crystallites, was calculated by using Eq. (10):

$$\psi = D_{BET}/D_{xrd} \quad (10)$$

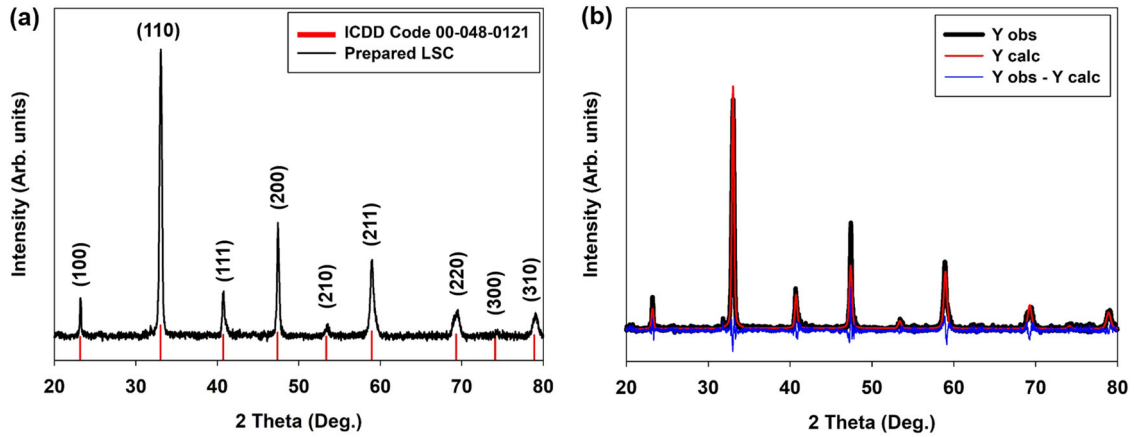

Fig. 2 XRD spectrum of the calcined $La_{0.6}Sr_{0.4}CoO_{3-\delta}$ powder at 900 °C: **a** Typical XRD and **b** Rietveld refinement patterns

The value provides an approximation of the average number of primary particles in the agglomerates and reflects the dispersibility of the prepared powder. The smaller the ψ value is, the better the dispersity of the powder is [20]. However, there is no particular range for the high or low value of ψ, since, based on the literature survey, very limited studies have reported this value. The calculated ψ value for the calcined LSC powder in this work is 5.33. It is higher than the reported ψ value in [21] for the $La_{0.6}Sr_{0.4}Co_{0.2}Fe_{0.8}O_{3-\delta}$ (LSCF) cathode calcined at 800 °C with a D_{BET} of 80 nm prepared by a microwave-assisted glycine-nitrate process ($\psi = 1.00$). The discrepancy between the ψ value is contributed by the different materials processing routes used to prepare the cathode materials and the difference in calcination temperatures required for the formation of a single-phase cathode material. Both factors significantly affect the microstructural properties of the produced materials.

The structural refinement of the XRD pattern of calcined LSC powder was carried out by Rietveld analysis, and the results are shown in Fig. 2b. The calculated pattern is comparable with the observed pattern, and the difference between these two patterns is very small and approximately a straight line. The goodness of the fit was 0.69. The value of the lattice parameter obtained after the refinement was 3.836 Å, which is comparable to the calculated value, i.e., 3.835 Å.

Figure 3 depicts a typical particle morphology of the calcined LSC powder. The calcined powder consists of homogeneous and regular shape particles. The particles are connected to each other and form hard agglomerates. This result is in line with the ψ value discussed earlier. The average particle size of the powder from the SEM measurements (D_{SEM}) and TEM measurements (D_{TEM}) are 219 ± 50 nm and 221 ± 40 nm, respectively. Although the D_{SEM} of the LSC powder produced in this work is larger than that of the LSC powder produced by a CA-EDTA sol-gel complexing method assisted with polyethylene glycol (PEG) as the surfactant in [14] and the LSCF powder produced by a modified sol-gel method assisted with AC as the dispersing agent in [7] at 60 nm and 35 nm, respectively, it has a larger specific surface area (9.87 $m^2 g^{-1}$) than these two powders (8.22 $m^2 g^{-1}$ and 9.50 $m^2 g^{-1}$, respectively). Therefore, from the results, it can be concluded that a large specific surface area of a powder produced by either sol-gel or modified sol-gel method can be obtained by employing suitable chemical agents such as a dispersing agent, i.e., AC, regardless of the particle size either in at the micro- or nanoscale. Table 1 shows the values of different parameters that were calculated based on the XRD, BET, SEM, and TEM analyses. As mentioned earlier, the synthesized LSC powder in this work could be used as the cathode for H^+-SOFC applications. Thus, the measurement of its electrical conductivity and electrochemical performance is necessary. The details of the results from the measurements are discussed in the following sections.

3.2 Electrical conductivity analysis

An appropriate (>100 S cm^{-1}) $\sigma_{d.c}$ is important for the practical application of the cathode to ensure efficient current collection. It is well known from the literature that Sr-doped lanthanum cobaltite, $La_{1-x}Sr_xCoO_{3-\delta}$ exhibits high electrical conductivity, which means it is essentially a *p*-type electronic conductor. The $\sigma_{d.c}$ measured on LSC is a sum of the electronic and oxide ion conductivities, owing to the co-presence of electron hole pairs and oxygen vacancies. However, it can be reasonably assumed that the measured $\sigma_{d.c}$ values are dominated by the electronic conductivity since the ionic conductivity in perovskite-type oxides materials is much lower than their electronic conductivity [22, 23].

The temperature dependence of $\sigma_{d.c}$ of the sintered LSC pellets measured in air is presented in Fig. 4a. The $\sigma_{d.c}$

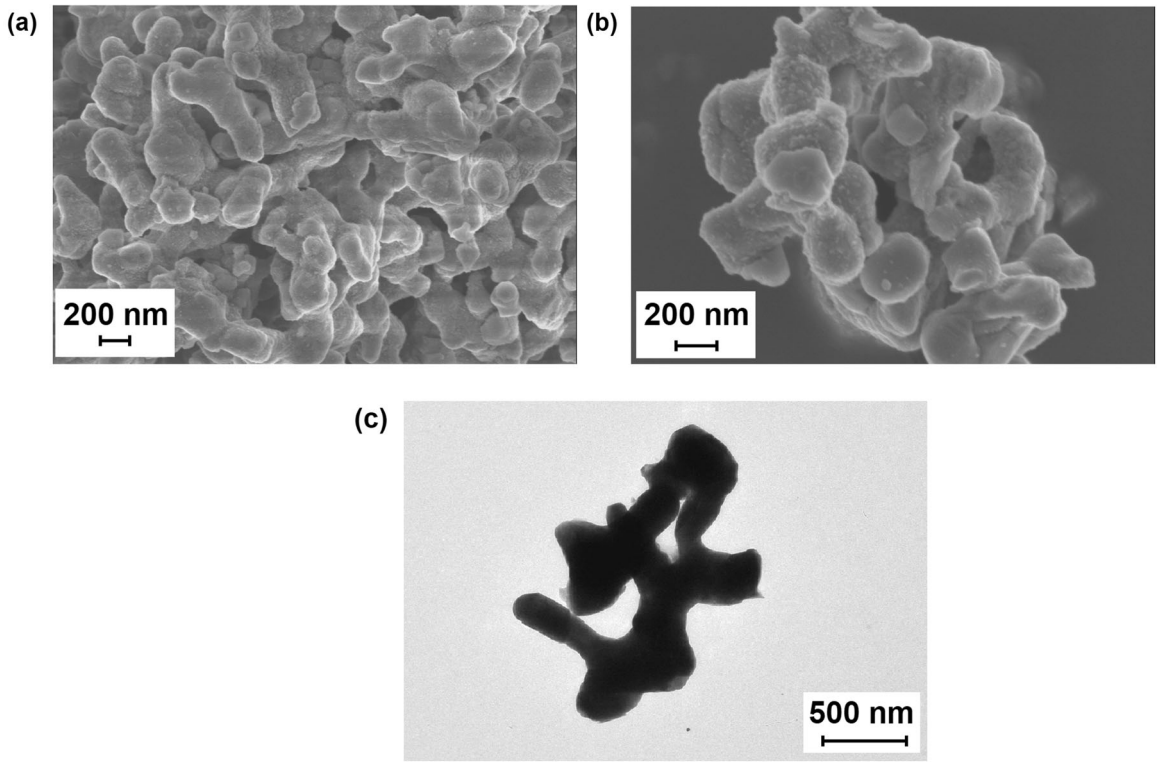

Fig. 3 Morphological images of $La_{0.6}Sr_{0.4}CoO_{3-\delta}$ powder after calcination at 900 °C captured by **a** FESEM at 30 kV; **b** FESEM at 50 kV, and **c** TEM at 10 kV

Table 1 Values for the various calculated parameters based on XRD, BET, SEM, and TEM analyses for $La_{0.6}Sr_{0.4}CoO_{3-\delta}$ calcined at 900 °C

a (Å)	ρ (g cm^{-3})	S_v (m^2 g^{-1})	D_{xrd} (nm)	D_{BET} (nm)	ψ	D_{TEM} (nm)	D_{SEM} (nm)
3.835	6.31	9.87	18	96	5.53	221 ± 40	219 ± 50

decreases with an increase in temperature from 400 °C to 800 °C for all pellets, indicating metallic-like behavior. The result is in agreement and comparable to the other reported studies in the literature [14, 17, 24–26]. Petrov et al. [27] reported that a decrease in the $\sigma_{d.c}$ of the LSC material with increasing temperature is due to the transition of the energy configuration from a low-to-high-spin state, which leads to a transition of localized electrons to itinerant electrons in trivalent cobalt ions (Co^{3+}). The transition is also due to an increase in the concentration of the tetravalent cobalt, Co^{4+} or oxygen vacancies. An increase in the oxygen vacancies breaks the Co-O-Co bonds, resulting in a further decrease in the $\sigma_{d.c}$.

Figure 4b shows the Arrhenius plots of ln (σT) vs. 1000/T for the LSC pellets after sintered at different sintering temperatures. It can be seen that there are changes in the slope at operating temperatures of 650–750 °C. The observation is in good agreement with the recent work performed by Wu et al. [17]. They reported that the changes are associated with the structural transformation of LSC from rhombohedral to cubic. This observation is also attributed to a transition from nearly pure electronic conduction to ionic conduction [28, 29] at the respective operating temperatures (650–750 °C). It is a proof that the LSC material is a type of mixed ionic-electronic conductor (MIEC), although it exhibited metallic-like behavior as previously mentioned. The E_a values in the temperature range from 500–600 °C of the sintered LSC pellets at 1000 °C, 1100 °C, and 1200 °C are 0.023 eV, 0.020 eV, and 0.049 eV, respectively. The values of E_a for the sintered LSC pellet at 1200 °C in this work is higher than the E_a value (0.028 eV) of the sintered LSC material ($T = 1200$°C) prepared by solid-state reaction method reported by Wu et al. [17] and the E_a value of the sintered LSC pellet at 1100 °C is lower than the E_a value (0.049 eV) of the sintered LSC material ($T = 1100$ °C) prepared by sol-gel technique as reported by Eslem Kisa and Demicran [30]. The variation in the E_a values is affected by the differences in the materials processing methods and microstructure. The small E_a value for the $\sigma_{d.c}$ expresses the small polaron-hopping mechanism enthalpy, suggesting that the material is a good cathode candidate for an intermediate temperature SOFC [30]. Although lower

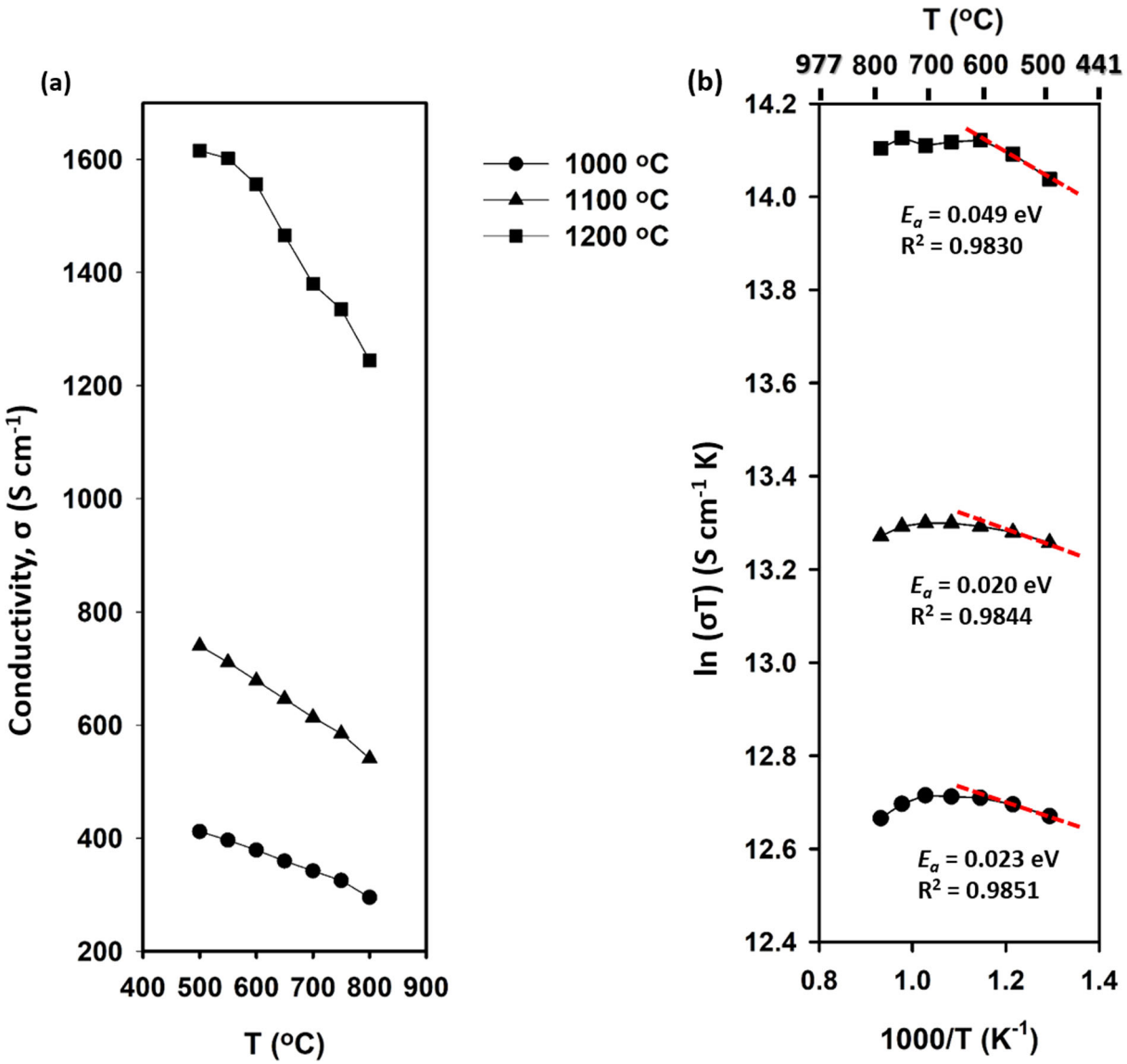

Fig. 4 D.C conductivities of the sintered $La_{0.6}Sr_{0.4}CoO_{3-\delta}$ pellets: **a** Plots of conductivity as a function of temperature and **b** Arrhenius plots of ln σT as a function of $1000/T$

E_a values were observed at sintering temperatures of 1000 °C and 1100 °C than at a sintering temperature of 1200 °C in this work, these temperatures are not suitable for the fabrication of a high-density LSC pellet. A high-density pellet is specifically required for the bulk conductivity measurements, as these measurements are greatly dependent on the properties of microstructure and fraction of pore volume [31].

The sintered LSC pellet at 1200 °C has the highest $\sigma_{d.c}$ values compared with the sintered LSC pellets at 1000 °C and 1100 °C. The high density (>95%) of the pellet sintered at 1200 °C, as shown in Table 2, contributed to the highest $\sigma_{d.c}$ values of the sample. The density is closely related to the porosity. A high-density sample means it has a reasonably low porosity, and the porosity knowingly affects the conductivity of a material. The porosity values of the sintered LSC pellets at 1000 °C, 1100 °C, and 1200 °C are 38.30%, 21.42%, and 4.85%, respectively. A decrease in porosity resulted in an increase in conductivity due to the decrease in pore-grain interface (effective contact area). The high existence or enlargement of the effective contact area amongst the particles or grains in a high-density specimen (low porosity) ensures the continuity of the electric path in the specimen by reducing internal blocking [31]. Conversely, poor contact amongst particles in a low-density specimen (high porosity) resulted in a decrease in the conductivity due to a discontinuity of the electric pathway in the specimen [29].

Table 2 Relative density of the various cathode materials prepared with different pressures, sintering temperatures, and soaking times

Cathode	Pressure	Sintering temperature (°C) and soaking time (*h*)	Relative density (%)	Reference
$La_{0.6}Sr_{0.4}CoO_{3-\delta}$	5 ton	1000 (2)	61.70	[This work]
		1100 (2)	78.58	
		1200 (2)	95.15	
$La_{0.6}Sr_{0.4}CoO_{3-\delta}$	300 MPa	1200/1250 (5)	Not mentioned	[14]
$La_{1-x}Sr_xCoO_{3-\delta}$	1 ton (uniaxially) and 325 MPa (isostatically)	1250 (4) and 1200 (16)	>99	[24]
$La_{0.6}Sr_{0.4}CoO_{3-\delta}$	Not mentioned	1200 (4)	>95	[26]
$La_{1-x}Sr_xCoO_{3-\delta}$	5 MPa	1150 (12)	>95	[25]
$La_{1-x}Sr_xCoO_{3-y}$	Not mentioned	1327–1427 (20–25)	92–98	[27]
$Ba_{1-x}La_xFeO_{3-\delta}$	200 MPa	1340–1370 (6)	Not mentioned	[32]
$SrCo_{0.9}Nb_{0.1}O_{3-\delta}$	Not mentioned	1100–1150 (10)	90–94	[22]
$La_{0.6}Ba_{0.4}Fe_{0.8}Ni_{0.2}O_{3-\delta}$	Not mentioned	1350 (6)	94.5	[33]
$La_{0.6}Sr_{0.4}Co_{0.2}Fe_{0.8}O_{3-\delta}$	Not mentioned	1200 (12)	Not mentioned	[34]

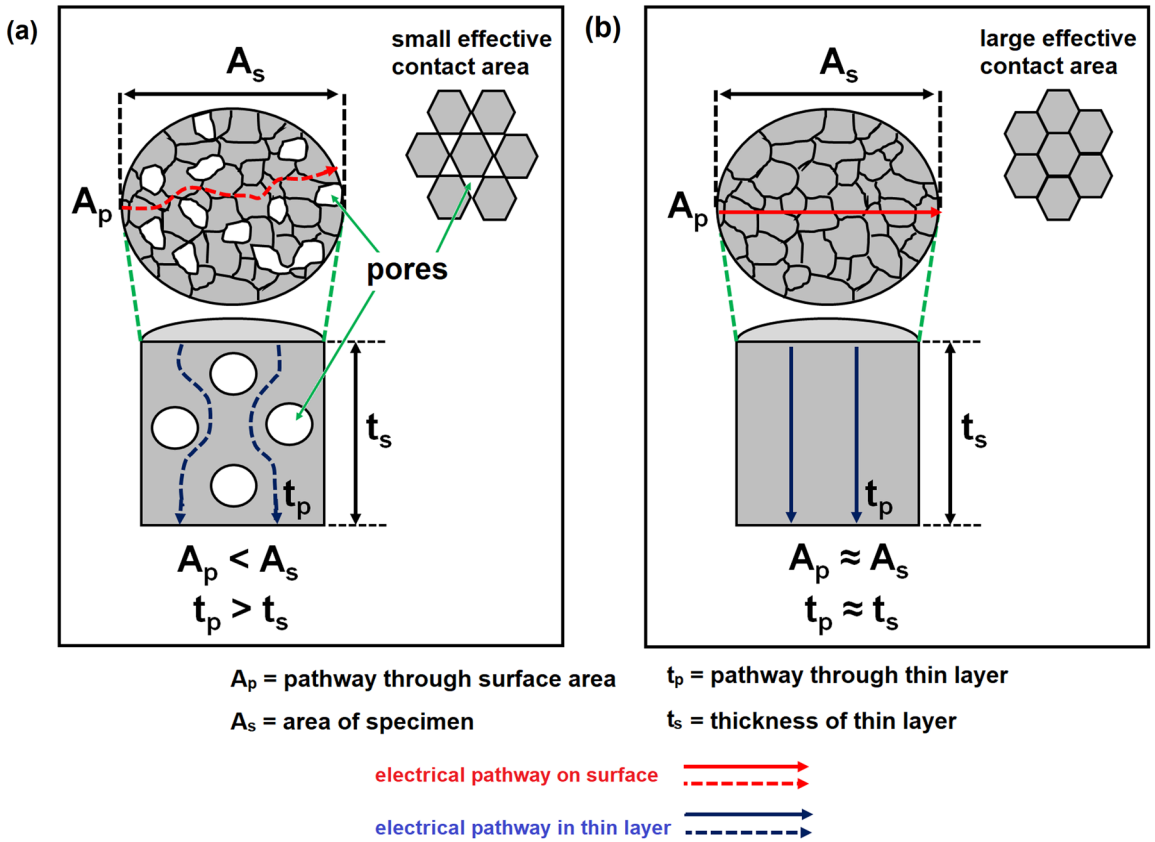

Fig. 5 Illustrations of the electrical pathway and effective contact area in **a** a porous pellet and **b** a highly dense pellet

Figure 5 depicts two simple illustrations to explain the difference in the electrical pathway and effective contact area of the high-porosity (low-density) and low-porosity (high-density) pellets. Assuming that both pellets have the same dimensions, the porous pellet in Fig. 5a has a smaller volume for the electrical current to pass through than does the highly dense pellet in Fig. 5b. Due to the presence of pores in the porous pellet, the effective contact area decreases, and the electrical pathway is either through the surface (area) or a thin layer (thickness) of the pellet (around the pores), making the pathway longer than its nominal dimension. A longer pathway with a small effective contact area creates high internal blocking, resulting in a higher resistivity with reduced conductivity. Conversely, with presumably no pores in a dense pellet, the enlargement of the effective contact area enables an electrical pathway

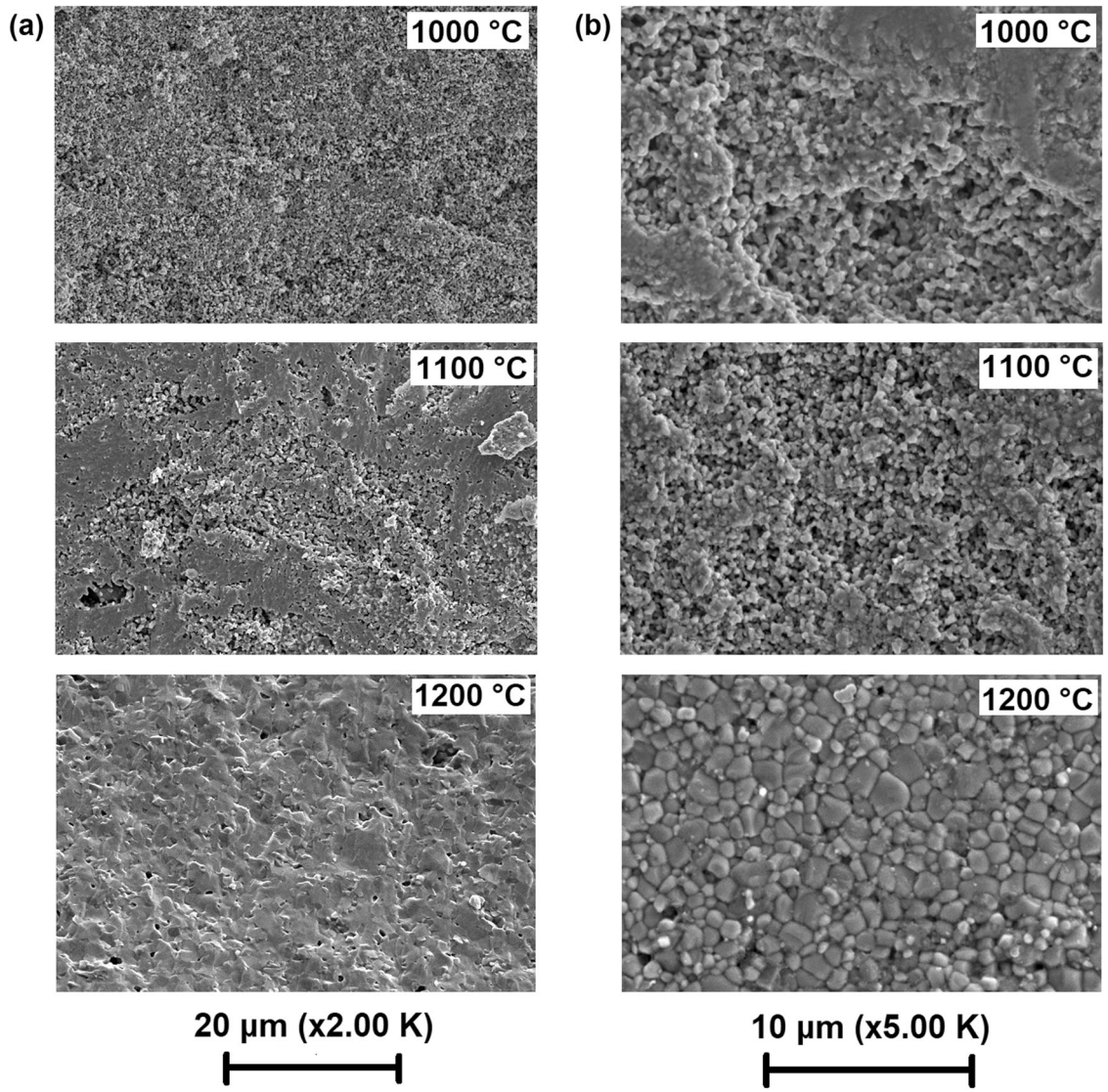

Fig. 6 SEM photographs of the **a** cross section and **b** surface of $La_{0.6}Sr_{0.4}CoO_{3-\delta}$ pellets after sintered at different temperatures

either on the surface or in the thin layer of the pellet within its nominal dimension [35].

It is well known that the density or microstructure (grain size, uniformity of grain, porosity, and boundary structure) of a pellet be adjusted by the means of the sintering temperature. Through a sequence of essential phenomena such as neck and pore formation, shrinkage, and grain growth, sintering facilitates the formation of a solid compact with a suitable microstructure. Both the densification through porosity elimination and grain growth occur simultaneously during the sintering process. The SEM images at the surfaces and cross sections of the fractured sintered LSC pellets at 1000, 1100, and 1200 °C are shown in Fig. 6. These results agree with the density values of each pellet (Table 2). As the sintering temperature increases, the pellets become denser and less porous, and the grain boundaries become clearer. Furthermore, the horizontal (diameter) and vertical (thickness) shrinkage percentage values of the sintered LSC pellets increase with increasing sintering temperatures, as shown in Fig. 7. This increase proves that the samples become more compact and denser as the sintering temperature increases. The shrinkage percentage values were calculated using Eqs. (11) and (12) as follows:

$$\text{Diameter shrinkage} = \left[\left(d_o - d_f\right)/d_o\right] \times 100\,\% \tag{11}$$

$$\text{Thickness shrinkage} = \left[\left(t_o - t_f\right)/t_o\right] \times 100\,\% \tag{12}$$

where d_o and t_o are the diameter and thickness before sintering, d_f and t_f are the diameter and thickness after sintering, respectively. Additionally, the highest density of

the sintered LSC pellet in this work was obtained at the lowest soaking time compared to the other reported studies in the literature (Table 2) for the $La_{1-x}Sr_xCoO_{3-\delta}$ and the other cathode materials [36, 37]. The highest compacting pressure applied in producing the green body of the pellet (pre-sinter pellet) in this work largely contributed to the high degree of adhesion amongst the adjacent particles or grains, the small pore size and more particle-to-particle contact points [33, 34]. Thus, only a short time was required for the transformation into a compact and denser pellet. In another work, Osman et al. [38] applied the same pressure in producing high-density ytterbium-doped barium cerate zirconate, $BaCeZrYbO_{3-\delta}$ electrolyte materials.

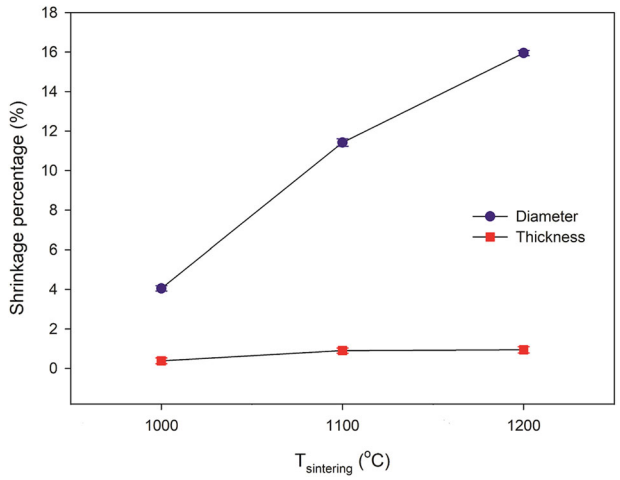

Fig. 7 Shrinkage percentage of the $La_{0.6}Sr_{0.4}CoO_{3-\delta}$ pellet after sintered at various temperatures

In this work, the LSC powder synthesized by a sol-gel method assisted by AC as the dispersing agent exhibits higher $\sigma_{d.c}$ values than the currently accepted $\sigma_{d.c}$ value of >100 S cm^{-1}. Thus, the synthesized LSC powder can be greatly regarded as a possible cathode material for IT-H^+-SOFC applications. However, further analysis of its potential to be used as a cathode material needs to be evaluated based on electrochemical performance.

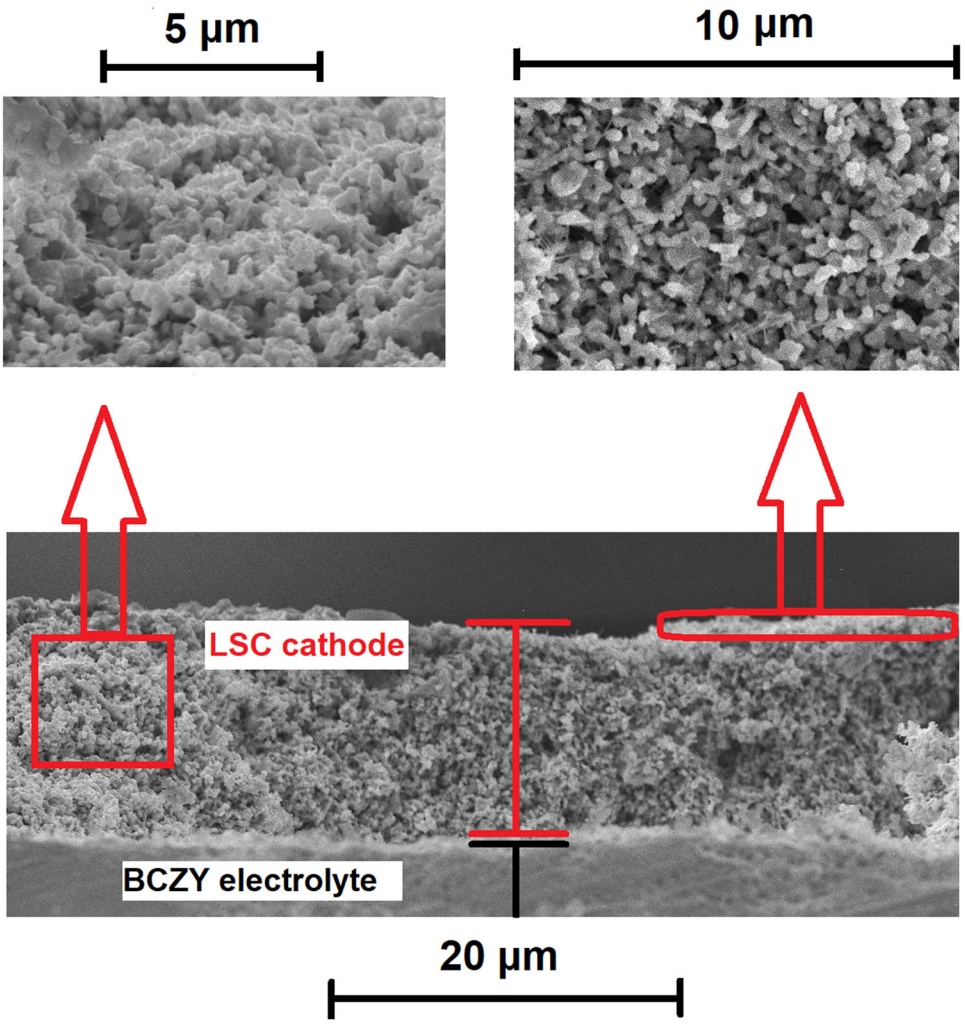

Fig. 8 SEM photograph at cross section of an LSC|BCZY|LSC symmetrical half-cell

3.3 AC impedance analysis

The screen-printed LSC film on the BCZY electrolyte was characterized by a.c electrochemical impedance spectroscopy. The fracture morphologies (cross section and surface) of the fabricated LSC|BCZY|LSC symmetrical half-cell of are shown in Fig. 8. An SEM image of the cell indicated that the sintering occurred between particles, forming sintering necks, where a homogenous and porous cathode microstructure (21%) was formed. The LSC cathode thin film with the thickness of 13 µm was also well-knitted with the BCZY electrolyte. The electrochemical properties of the cell were studied at temperatures of 500–800 °C, and the corresponding typical a.c impedance spectra are shown in Fig. 9. There are at least two arcs in the a.c impedance spectra, which indicate that the two responses corresponding to the electrolyte and/or cathode reactions occurred. The cathode reactions include the reduction of molecular oxygen to oxygen ions, surface adsorption, gas diffusion, dissociation, and charge transfer [25, 39]. The overall length of the impedance arcs decreases as the temperature increases, indicating that the polarization resistance (R_p) or ASR decreased. The ASR values obtained from this work are 5.0 Ω cm^2, 4.0 Ω cm^2, 3.25 Ω cm^2, 1.7 Ω cm^2, 0.55 Ω cm^2, 0.14 Ω cm^2, and 0.06 Ω cm^2 at temperatures of 500 °C, 550 °C, 600 °C, 650 °C, 700 °C, 750 °C, and 800 °C, respectively. Figure 10 shows an example of the equivalent circuit model used for the fitting process. L accounts for the inductance of the wiring used for the impedance measurement. *Rs, R1*, *R2*, and *R3* are resistances, and *Q1*, *Q2*, and *Q3* are constant phase elements or can also be regarded as pseudo-capacitances. The high-frequency intercept of the impedance spectra is attributed to the ohmic resistance (R_Ω). Meanwhile, the low-frequency intercept of the impedance spectra corresponds to the total cell resistance (R_T). The difference between the high and low frequencies intercepts represents the total R_p.

Based on the ASR data, an Arrhenius plot of the ln ASR vs. 1000/*T* is plotted, as shown in Fig. 11. From the plot, it can be seen that there are changes in the slope at operating temperatures of 650–800 °C. This observation is in agreement with the results of electrical conductivity analysis. As mentioned earlier, the changes are associated to the structural transformation from rhombohedral to cubic phase and transition from pure electronic conduction to ionic conduction. Increasing in ionic conduction led to better electrochemical performance of the material as it is well known that the electrochemical performance of an electrode material is greatly affected by the ionic conduction rather than electronic conduction. Thus, the ASR values (0.06–1.70 Ω cm^2) at the operating temperatures of 650–800 °C is lower than the ASR values (3.25–5.00 Ω cm^2) at the operating temperatures of 500–600 °C. The activation energy E_a values obtained from the plot are 0.25 eV (500–600 °C) and 1.94 eV (650–800 °C), respectively. The range of these E_a values is larger than the range of reported E_a values (1.10–1.76 eV) for LSC and LSC composite materials [3, 39–41]. The variation in the E_a values is contributed by the difference in the temperature range used to fit the ASR data in the Arrhenius plot. The ASR values obtained from this work are comparable with those ASR values reported in the literature, as shown in Table 3. The discrepancies in the ASR values are mainly due to the processing and fabrication of the materials, as well as the type of working electrolyte used. Different processing and fabrication techniques provide different microstructural properties of the cathode materials, which in turn affect their electrochemical performance, as recently reported by Muhammed Ali et al [21, 42] and Zeng and Huang [43].

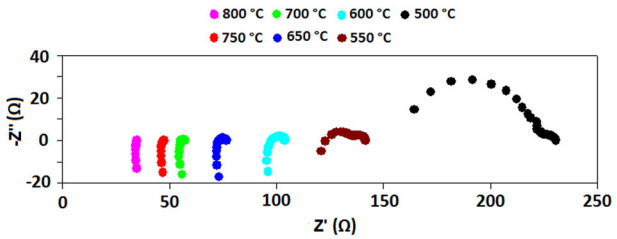

Fig. 9 Typical a.c impedance spectra of an LSC|BCZY|LSC symmetrical half-cell measured at various temperatures

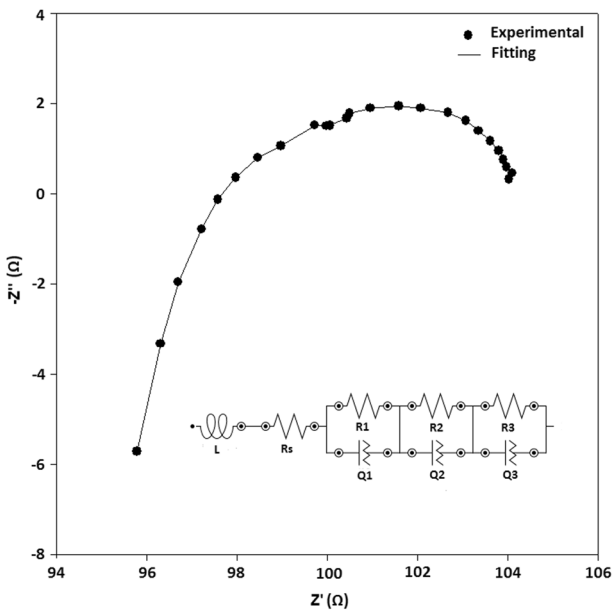

Fig. 10 Experimental and fitting results of an a.c impedance spectrum measured at 600 °C

From the a.c impedance analysis, the relatively low values of ASR at 650–800 °C indicated that the utilization of the LSC powder synthesized by a sol-gel method assisted with AC as the dispersing agent in the fabricated BCZY electrolyte-based symmetrical cell is preferred for practical applications of an IT-H^+-SOFC. However, to further enhance the electrochemical performance by reducing the ASR values of the synthesized LSC cathode material, a novel work was successfully conducted to improve its microstructural properties by combining EG and AC as a combined surfactant-dispersing agent. The effects of the microstructural properties on the d.c conductivity and electrochemical performance of the powders are under thorough investigation, and the results will be reported elsewhere.

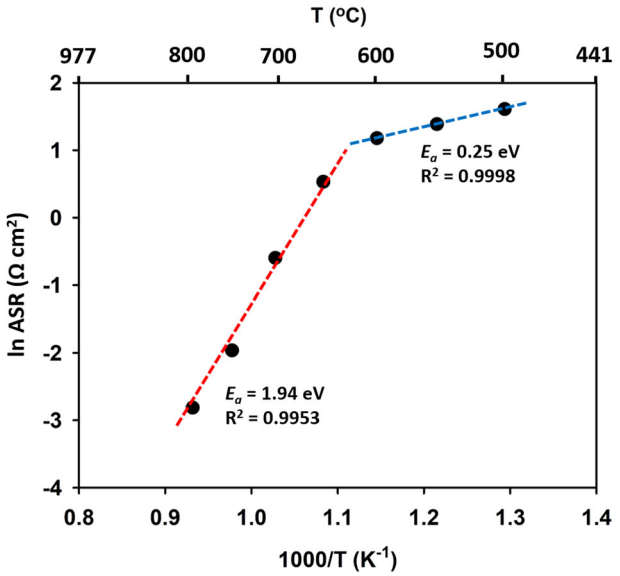

Fig. 11 Arrhenius plot of temperature (1000/*T*) dependence of the area specific resistance (ln ASR) of the $La_{0.6}Sr_{0.4}CoO_{3-\delta}$ cathode

4 Conclusions

In this work, submicron single-phase LSC powder synthesized via a modified citrate-EDTA sol-gel method assisted with AC as a dispersing agent showed good potential as a cathode material for H^+-SOFC applications based on a proton conductor of $BaCe_{0.54}Zr_{0.36}Y_{0.2}O_{2.95}$ (BCZY) at intermediate temperatures. Different microstructural properties (density and porosity) of the bulk LSC samples sintered at various temperatures had a significant effect on the $\sigma_{d.c}$ of the samples. Increases in the sintering temperature led to a decrease and an increase in the porosity and density of the sintered pellets, respectively. A relatively high dense and low porosity of LSC pellet sintered at 1200 °C exhibited the highest $\sigma_{d.c}$ value due to the continuity of the electrical pathway throughout the large effective contact area in the sample. The electrochemical performance in terms of the ASR of the synthesized LSC material coupled with a BCZY electrolyte decreased from 5.0 Ω cm^2 at 500 °C to 0.06 Ω cm^2 at 800 °C. These values are comparable to the electrochemical performance of the LSC material coupled with other electrolyte materials. Further studies related to the microstructural modification

Table 3 ASR values of the LSC cathode with various electrolytes measured at various temperatures

Synthesis method	Fabrication method	Electrolyte	ASR (Ω cm^2)	Reference
Modified sol-gel	Screen-printing	BCZY	3.25 (600 °C)	[This work]
			0.55 (700 °C)	
			0.06 (800 °C)	
Commercial powder	Pulsed laser deposition	YSZ	4.0 (600 °C)	[1]
			0.3 (700 °C)	
Infiltration of nitrates	Infiltration into porous backbone	$BaCe_{0.2}Zr_{0.7}Y_{0.1}O_{3-\delta}$	0.062 (600 °C)	[4]
Polymeric complexation	Hand-painting	BCZY	0.97 (600 °C)	[12]
			0.48 (700 °C)	
Glycine-nitrate	Screen-printing	GDC	12.0 (600 °C)	[44]
			2.0 (700 °C)	
			0.35 (800 °C)	
Salt assisted spray pyrolysis	Spin-coating	YZS	5.54 (600 °C)	[45]
Flame spray deposition	Spray deposition	$Ce_{0.8}Gd_{0.2}O_{1.9-\delta}$ (CGO)	0.96 (600 °C)	[46]
Solid state reaction	Screen-printing	SDC20	1.08 (600–700 °C)	[17]

of the LSC material to enhance its electrochemical performance are planned.

5 Disclaimer

I can confirm that this is our original unpublished work, and that it has not been submitted to any other journals for publication. We declare that the article is original. The results/data in this article are from our original work and have not been published elsewhere. The article has been written by the stated authors (Abdullah Abdul Samat, Abdul Azim Jais, Mahendra Rao Somalu, Nafisah Osman, Andanasturi Muchtar, and Kean Long Lim) who are all aware of its content and approve its submission. The journal policies have been reviewed. The article has been 'spell checked' and 'grammar checked'. The article is only submitted to the journal of Sol-Gel Science and Technology for consideration and possible publication and the submitted article is not under consideration for publication elsewhere. If the article is accepted to be published in the journal of Sol-Gel Science and Technology, we agree that the article will not be published elsewhere in the same form, in English or in any other languages, without the written consent of the Publisher

Acknowledgements The authors would like acknowledge the Research University grant (DIP-2016-005) provided by Universiti Kebangsaan Malaysia. Also, the authors would like to thank the Ministry of Higher Education (MOHE) of Malaysia for financial support provided via the Transdisciplinary Research Grant Scheme (600-IRMI/TRGS 5/3 (1/2016)-2) and the Fundamental Research Grant Scheme (FRGS/2/2014/ST05/UKM/03/1). Abdullah Abdul Samat thankfully acknowledges the MOHE and Universiti Malaysia Perlis (UniMAP) for the SLAB/SLAI PhD scholarship. Facilities support from the Centre for Research and Instrumentation Management (CRIM) of Universiti Kebangsaan Malaysia, Universiti Tun Hussein Onn Malaysia (UTHM), and Universiti Teknologi MARA is also appreciatively acknowledged.

Compliance with ethical standards

Conflict of interest The authors declare that they have no conflict of interest.

References

1. Garbayo I, Esposito V, Sanna S, Morata A, Pla D, Fonseca L, Sabate N, Tarancon A (2014) J Power Sources 248:1042–1049
2. Heel A, Holtappels P, Graule T (2010) J Power Sources 195:6709–6718
3. Hayd J, Dieterle L, Guntow U, Gerthsen D, Ivers-Tiffée E (2011) J Power Sources 196:7263–7270
4. Samson AJ, Søgaard M, Bonanos N (2012) Electrochem Solid-State Lett 15:B54–B56
5. Ricote S, Bonanos N, Rørvik PM, Haavik C (2012) J Power Sources 209:172–179
6. Promsuy S, Tangtrakarn A, Mongkolkachit C, Wanakitti S, Amornkitbamrung V (2016) J Sol-Gel Sci Technol 78:187–194
7. Ismail I, Osman N, Md Jani AM (2016) J Sol-Gel Sci Technol 80:259–266
8. Ghouse M, Al-Yousef Y, Al-Musa A, Al-Otaibi MF (2010) Int J Hydrog Energy 35:9411–9419
9. Abdul Samat A, Somalu MR, Muchtar A, Osman N (2016) Malays J Anal Sci 20:1458–1466
10. Abdul Samat A, Somalu MR, Muchtar A, Osman N (2016) Solid State Sci Technol 24:135–142
11. Kim JH,Park YM,Kim H,(2011) J Power Sources 196:3544–3547
12. Abdul Samat A, Somalu MR, Muchtar A, Hassan OH, Osman N (2016) J Sol-Gel Sci Technol 78:382–393
13. Naceur H, Megriche A, El Maaoui M (2014) J Adv Ceram 3:17–30
14. Tao Y, Shao J, Wang J, Wang WG (2008) J Power Sources 185:609–614
15. Baharuddin NA, Muchtar A, Somalu MR, Seyednezhad M (2017) Powder Technol 313:382–388
16. Bansal NP, Zhong Z (2006) J Power Sources 158:148–153
17. Wu YC, Huang PY, Xu G (2017) Ceram Int 43:2460–2470
18. Nicole ML, Closset NP, van Doorn RHE, Kruidhof H, Boeijsma J (1996) Powder Diffr 11:31–34
19. Anwar M, Muhammed Ali SA, Abdalla AM, Somalu MR, Muchtar A (2017) Process Appl Ceram 11:67–74
20. Li S, Ma P, Zhu X, Jiang N, Ivanov M, Li C, Xie T, Kuo H, Shi Y, Chen H, Pan Y, Hreniak D, Li J (2017) Ceram Int 43:10013–10019
21. Muhammed Ali SA, Anwar M, Baharuddin NA, Somalu MR, Muchtar A (2018) J Solid State Electrochem 22:263–273
22. Zhang L, Long W, Jin F, He T (2013) Int J Hydrog Energy 38:7947–7956
23. Bai Y, Liu M, Ding D, Blinn K, Qin W, Liu J, Liu M (2012) J Power Sources 205:80–85
24. Søgaard M, Hendriksen PV, Mogensen M, Poulsen FW, Skou E (2006) Solid State Ion 177:3285–3296
25. Gwon O, Yoo S, Shin J, Kim G (2014) Int J Hydrog Energy 39:20806–20811
26. Egger A, Bucher E, Yang M, Sitte W (2012) Solid State Ion 225:55–60
27. Petrov AN, Kononchuk OF, Andreev AV, Cherepanov VA, Kofstad P (1995) Solid State Ion 80:189–199
28. Ritcher J, Holtappels P, Graule T, Nakamura T, Gauckler LJ (2009) Mon Chem 140:985–999
29. Paydar S, Shariat MH, Javadpour S (2016) Int J Hydrog Energy 41:23145–23155
30. Eslem Kisa A, Demircan O (2017) J Sol-Gel Sci Technol 82:352–362
31. El Khal H, Cordier A, Batis N, Siebert E, Georges S, Steil MC (2017) Solid State Ion 304:75–84
32. Montes JM, Cuevas FG, Cintas J (2008) Appl Phys A 92:375–380
33. Seyednezhad M, Rajabi A, Muchtar A, Somalu MR, Ooshaksaraei P (2017) J Asian Ceram Soc 5:77–81
34. Zhang X, Gao H, Zhang Z, Wen R, Wang G, Mu J, Che H, Zhang X (2017) Ceram Int 43:6345–6352
35. Osman N, Talib IA, Hamid HA (2009) Sains Malays 38:103–107
36. Ding X, Gao X, Zhu W, Wang J, Jiang J (2014) Int J Hydrog Energy 39:12092–12100
37. Xiao J, Yuan H, Chen L, Xiong C, Liu W (2015) Ionics 21:1193–1199
38. Jun A, Yoo S, Gwon O, Shin J, Kim G (2013) Electrochim Acta 89:372–376
39. Peng B, Chen G, Wang T, Zhou J, Guo J, Cheng Y, Wu K (2012) J Power Sources 201:174–178
40. Wang MS, Wang JX, He CR, Xue YJ, Miao H, Wang Q, Wang WG (2015) Ceram Int 41:5017–5025

41. Hu Y, Bouffanais Y, Almar L, Morata A, Tarancon A, Dezanneau G (2013) Int J Hydrog Energy 38:3064–3072
42. Muhammed Ali SA, Anwar M, Somalu MR, Muchtar A (2017) Ceram Int 43:4647–4654
43. Zeng R, Huang Y (2017) Int J Hydrog Energy 42:7220–7225
44. Zhao F, Peng R, Xia C (2008) Fuel Cells Bull 2008:12–16
45. Benel C, Darbandi AJ, Djenadic R, Evans A, Tolke R, Prestat M, Hahn H (2013) J Power Sources 229:258–264
46. Karageorgakis NI, Heel A, Bieberle-Hütter A, Rupp JLM, Graule T, Gauckler LJ (2010) J Power Sources 195:8152–8161